Desalination and Water Treatment
www.deswater.com

doi: 10.5004/dwt.2017.21748

100 (2017) 100–115
December

Comparison of the efficiency of graphene oxide, activated graphene oxide, dendrimer-graphene oxide and activated dendrimer-graphene oxide for nitrate removal from aqueous solutions

Abolghasem Alighardashi[a], Zahra Kashitarash Esfahani[a,*], Abbas Afkhami[b], Farhood Najafi[c], Nemat Hassani[d]

[a]*Faculty of Civil, Water and Environmental Engineering, Shahid Beheshti University, P.O. Box 16765-1719, Tehran, Iran, email: a_ghardashi@sbu.ac.ir (A. Alighardashi), health.engineering@gmail.com (Z. Kashitarash Esfahani)*
[b]*Faculty of Chemistry, Bu-Ali Sina University, Hamadan, Iran, email: afkhami@basu.ac.ir*
[c]*Institute of Color Science and Technology, Tehran, Iran, email: farhoodnajafi@yahoo.com*
[d]*Faculty of Civil, Water and Environmental Engineering, Shahid Beheshti University, Tehran, Iran, email: Nemathassani@yahoo.com*

Received 1 December 2016; Accepted 1 December 2017

ABSTRACT

This study determined the nitrate removal efficiency of graphene oxide (GO), activated GO (AGO), dendrimer-graphene oxide (PAMAM-GO) and activated PAMAM-GO (A PAMAM-GO) for the first time in the world. Field emission scanning electron microscopy (FESEM) with EDS and Fourier transform infrared spectroscopy (FTIR) were used to characterize the nanostructures. Experiments were performed in a batch reactor. Results showed that GO, PAMAM and PAMAM-GO could not serve as effective materials for nitrate removal. The efficiency of GO and PAMAM was developed by activation and composition so that 0.4 g/l AGO removed 80% of the nitrate in 40 min at a pH of 7.5. The highest removal efficiency was obtained with A PAMAM-GO. By some characterizations using EDS and FTIR as well as according to the functionalized using hydrochloric acid, we understand that the ion exchange between nitrate and chloride is the main mechanism of nitrate removal by AGO and A PAMAM-GO.

Keywords: Graphene oxide; Activation; Nitrate; Removal; PAMAM

1. Introduction

In recent years, nitrate contamination in surface and groundwaters has been a serious ecological problem worldwide. Nitrate has been found in water contaminated by sanitary, industrial, and agricultural wastewater. Methemoglobinemia (baby blue syndrome) and eutrophication of surface water resources are examples of the adverse effects of nitrates [1,2]. Metals reduction, enzymes, ion exchange, reverse osmosis (RO), electrodialysis (ED) and absorption are proper physical and chemical methods for nitrate removal. The high energy costs and the high volume of brine waste produced are problems relating to RO and ED [3]. Biological denitrification is more practical and economical than chemical and physical methods but has limitations. These include the need for an additional carbon source for microorganisms, production of pollutants (bacterial products, sludge), and the need for special treatment methods [3,4].

Nanomaterials are currently considered to treat and remove pollutants from the environment. Nanoparticles have a much wider surface area than larger particles and can interact with various chemical groups to enhance their affinity to a particular compound. Research has focused on the use of nanotechnology to purify and remove contaminants from the environment [5,6]. Carbon-based

*Corresponding author.

nanomaterials have been shown to be an important class of materials for environmental applications. Graphene (G) and its oxidized derivatives, graphene oxide (GO), as new allotropes of carbon, have been proposed as adequate and effective solution to solve environmental problems. Graphene is a two-dimensional sheet of carbon atoms in a hexagonal configuration with a large specific surface area of over 2600 $m^2 g^{-1}$ [7,8].

Carbon atoms in graphene bond with SP^2 hybrids. A carbon atom in a graphene layer has an outside orbital. This orbital is a good place to bond with certain functional groups and hydrogen atoms. The bond between carbon atoms on a sheet is a very strong covalent bond [8–10]. It appears that the small size and other features of graphene have the potential for *in situ* treatment of contaminated water [9,11]. Removal mechanisms of graphene include redox reactions, adsorption, nano-catalysis, and nano-photo catalysis [12].

Kumar et al. developed an amine-treated GO adsorbent for removal of chromium (VI) [13]. The absorption of Cu(II) by sulfonated magnetic GO composites has also been studied [14]. Similar research has shown that GO is a highly effective absorbent for Zn(II) removal from aqueous solutions [15], decontamination of wastewater and waste gas and hydrogen storage/generation [16], oil spill cleanup in water [17] energy storage and conversion to an electrochemical sensor [18]. The use of graphene for nitrate removal has not been successful thus far. Motamedi showed that only 7% of the nitrate could be removed after 48 h by raw GO. It is necessary to use other nanomaterials such as iron nanoparticles to enhance the efficiency of GO [19].

Nowadays, dendrimer nanostructures are considered in many areas of biomedical and environmental fields. Dendrimers are capable of locking different molecules in their branches. They carry a variety of molecules by the existence of multiple functional groups on their surface. Non-toxic, eco-friendliness and biodegrability are among important features of these compounds. Polyamidoamine (PAMAM) and polypropylenimine (PPI) are the most important dendrimers that are available commercially. The most important application of PAMAM and PPI is their biocompatibility [20–22]. The study on the removal of organic contaminants and dyes from textile wastewater using PPI dendrimers showed that it could be used for dye removal from textile wastewater [20]. Hayati et al. have shown that pH_{pzc} and maximum adsorption capacity for DB78 and DR80 of dendrimer-Titania nanocomposite are 4.6, 990 mg/g and 1250 mg/g, respectively [20]. Moses Sadeghi et al. have reached 97–99% removal efficiency for color removal and stated that kinetics adsorption isotherm followed the Languir model [21]. In addition, Ilaiyaraja et al. obtained 0.355 g adsorption capacity of cobalt in pH = 4.5 [23].

With regard to the carried out investigations, no studies have been developed concerning the possibility of nitrate removal from aquatic environments by composition materials such as dendrimers and graphene. Due to severity of nitrate contamination and its dangers, such studies are extremely important.

The current study determined the effectiveness of GO, AGO, PAMAM, PAMAM-GO nanocomposite and A PAMAM-GO nanocomposite (novel structures of GO and PAMAM) for nitrate removal from aquatic environments. Lack of prior research on activation of GO and A PAMAM-GO prompted this study on the development and modification of the new structure of GO and PAMAM-GO nanocomposite. These materials have been produced for the first time in the world and used for nitrate removal from aqueous solutions in this research.

2. Experimental

2.1. Materials and chemicals

GO was synthesized using the modified Hummers method [24,25] from natural graphite powder. Fig. 1 presents images and characteristics of the GO synthesis.

Polyamide amine dendrimer, the second generation (PAMAM-G2) was synthesized according to the methods mentioned in the previous studies [26].

Sodium nitrate, sodium hydroxide, and hydrochloric acid were purchased from Merck (Germany) and used without pre-treatment.

2.2. Instrumentation

The pH was measured using a Jenway pH meter (model 3510). A UV-visible spectrophotometer (UV mini 1240; Shimadzu) at wavelengths of 220 and 275 nm was used to measure the nitrate concentration. A digital scale (Sartorius Xpert Pro) with an accuracy of 4×10^{-4} g was used to weigh the substances. A magnetic stirrer (MR Hei-Standard; Heidolph) at set speed was used for mixing. Nano-composites were synthesized by ultrasonic (model up400s), memmert oven and stoves devices. FE-SEM images of the AGO and A PAMAM-GO samples were prepared using a field-emission scanning electron microscope (Sigma; Zeiss; Germany) and using an EDS and map detector (Oxford Instruments). Morphology of AGO and A PAMAM-GO was evaluated at magnifications of kX 00.1 to kX 00.50.

2.3. Activation of Graphene Oxide (GO)

Hydrochloric acid was used to activate the GO. 5 g of synthesized graphene oxide mixed with 20% hydrochloric acid for 20 min at 500 rpm (Fig. 2). It was dried for 12 ± 2 h

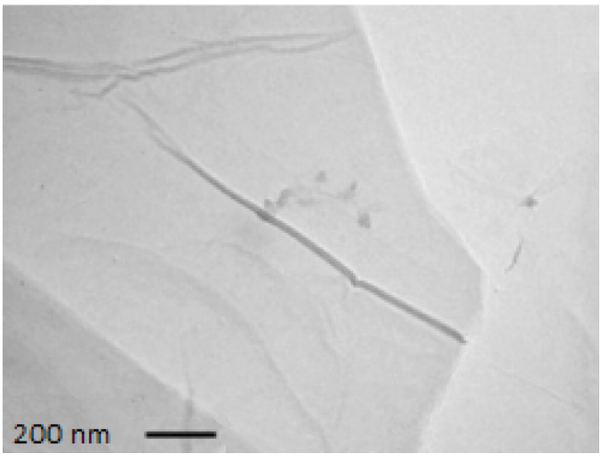

Fig. 1. TEM image of GO (before activation).

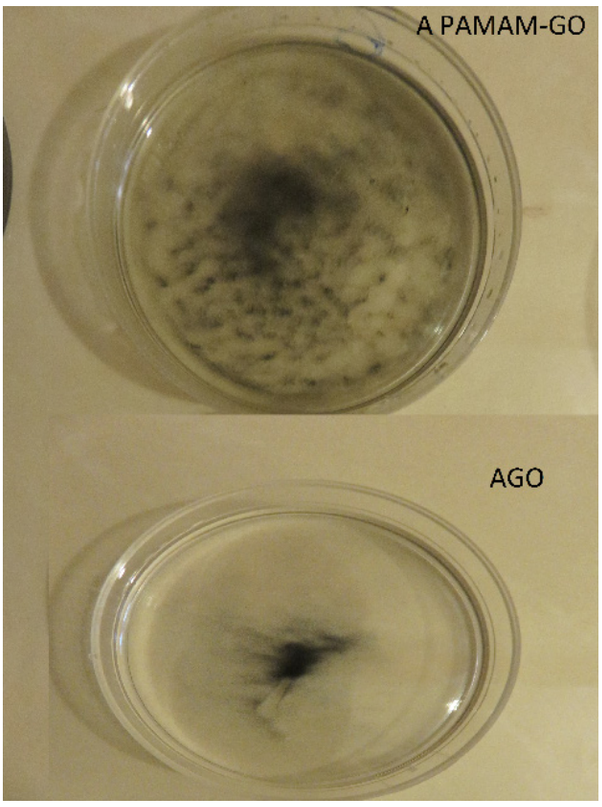

Fig. 2. Image of functionalized graphene oxide (GO) and dendrimer-graphene oxide (PAMAM-GO).

in an oven at a temperature of 140 ± 10°C and then placed in the furnace for 6 h at 450 ± 50°C.

2.4. Synthesis and activation of dendrimer-graphene oxide (PAMAM-GO) nanocomposite

10cc of PAMAM-G2 (10% weight by volume) with 0.02 g of GO was ultrasonic for 12 min to produce PAMAM-GO nanocomposite. It was functionalized using 20% hydrochloric acid for 25 min at 500 rpm speed (Fig. 2). It was dried for 12 ± 2 h in an oven at a temperature of 140 ± 10°C and then activated in the furnace for 6 h at 450 ± 50°C.

2.5. Batch experiments

A stock solution of nitrate was prepared by dissolving potassium nitrate in distilled water. All experiments were conducted in a batch reactor at an ambient air and at room temperature. The effective factors investigated were pH (4, 7.5, 9), contact time (5–65 min), nitrate concentration (45, 75, 110 mg/l), GO and AGO concentrations, (0.27, 0.4, 0.75 and 1 g/l), PAMAM-GO concentration (3, 5 and 10 ml/l) and A PAMAM-GO concentration (0.008, 0.017, 0.025, 0.033 g/l). Testing varied the values for one factor, while the other factors were held constant to evaluate the effectiveness and efficiency of each factor. NO_3 was determined according to standard methods No.4500B [27]. To increase the reliability, accuracy and precision testing, sampling, and analysis of samples at each stage, the operation was repeated three times.

Removal efficiency at different stages was calculated using the results and initial concentrations as:

$$E = \frac{C_i - C_f}{C_i} \times 100 \quad (1)$$

where C_i and C_f are the initial and final concentrations of NO_3, respectively.

The optimum values of each variable were selected, and performance of GO, AGO, PAMAM, PAMAM-GO nanocomposite and A PAMAM-GO nanocomposite was evaluated by using SPSS-16 software.

2.6. Isotherms and modelling of nitrate absorption kinetics

The linear form of the Langmuir, Freundlich, Temkin, and Elovich models and the equations of the pseudo-first, pseudo-second order and intraparticle diffusion kinetic models were used to analyse nitrate absorption by A GO/PAMAMs nanocomposite. The amount of adsorbed ions at equilibrium time (mg/g) is denoted as q_e and is defined as:

$$q_e = \frac{C_0 - C_e}{m} \times v \quad (2)$$

where C_0 is the initial concentration of contaminant (mg/l), m is the adsorbent weight (g), v is the volume of solution (l), and C_e is adsorbing material equilibrium concentration in the solution phase after absorption (mg/l).

3. Results and discussion

3.1. Characterization of AGO

Fig. 3 and Fig. 4 show the AGO images. Fig. 4 shows that synthesized GO was multiple layers. New species are observed on the surface of AGO that are related to the chloride ions. EDS spectrum analysis of the AGO samples revealed that the oxygen and chloride contents were 45.8% and 1.2% in mass, respectively. Furthermore, covalent bonding is further proved by FTIR spectroscopy (Fig. 9).

3.2. Characterization of A PAMAM-GO

The FE-SEM images in Fig. 5 and TEM images in Fig. 6 show the A PAMAM-GO nanocomposite. Compared to the relatively smooth surface of AGO and GO, new species are observed on the surface of A PAMAM-GO nanocomposite that are related to the PAMAM. Images in Fig. 5 and Fig. 6 show that PAMAM branches are well dispersed on the surface of GO nanosheets with an average particle size of 20 nm. Its covalent bonding is further proved by FTIR spectroscopy (Fig. 10).

EDS spectrum analysis of the A PAMAM-GO samples revealed that the oxygen and chloride contents were approximately 20% and 0.4% in mass, respectively (Fig. 10).

This amount of oxygen-containing indicates that different functional groups on the surface of A PAMAM-GO exist. Identification of chloride ion confirms the activation of PAMAM-GO by HCl. These are also confirmed by FT-IR analysis [28].

Fig. 3. FE-SEM images of activated graphing oxide (AGO).

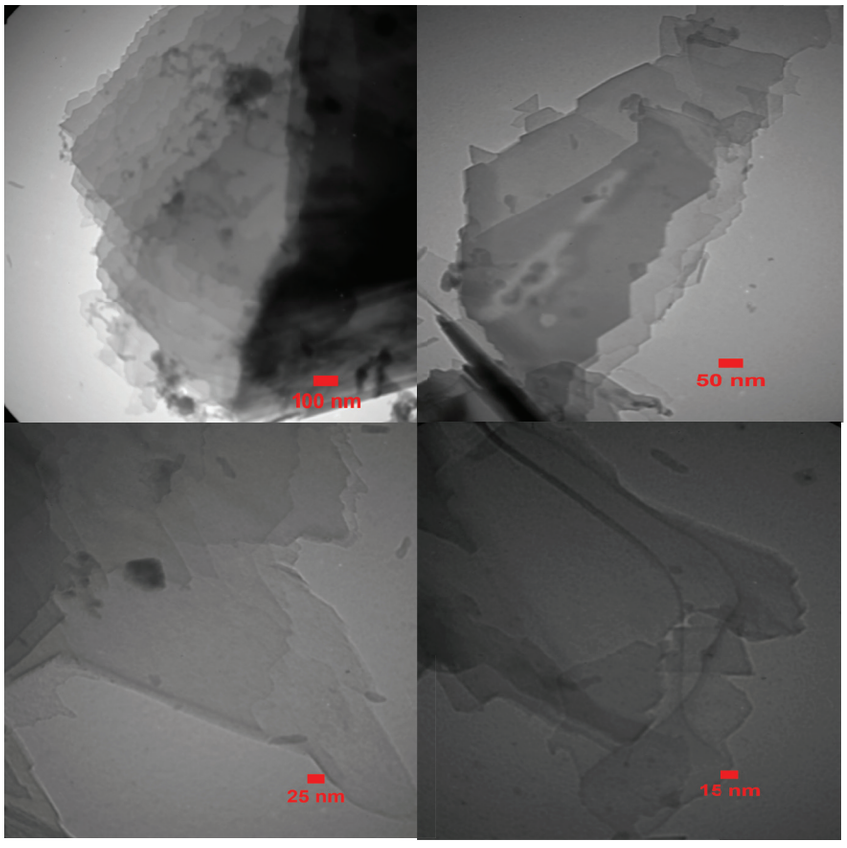

Fig. 4. TEM images of AGO.

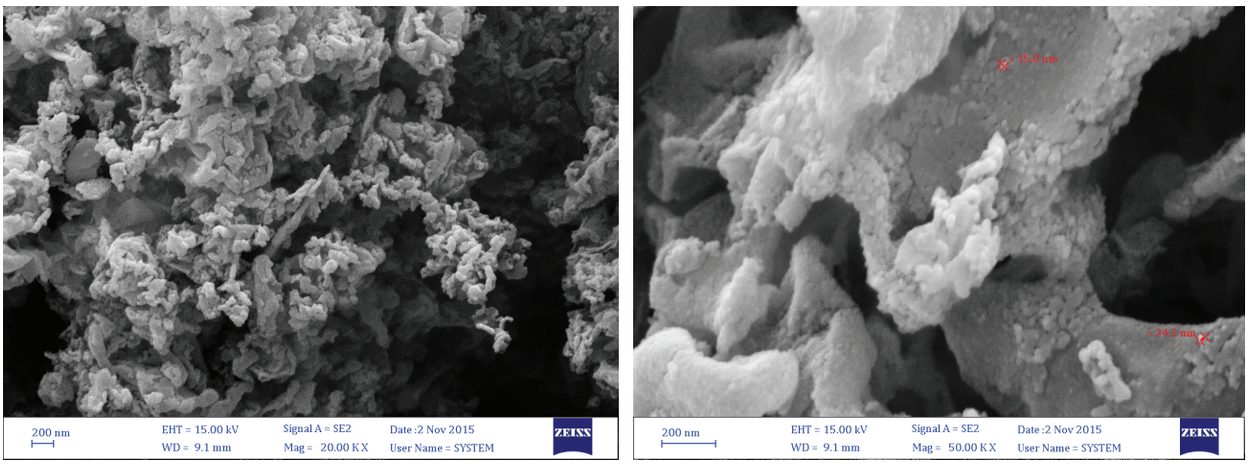

Fig. 5. FE-SEM images of activated dendrimer-graphene oxide (A PAMAM-GO) nanocomposite.

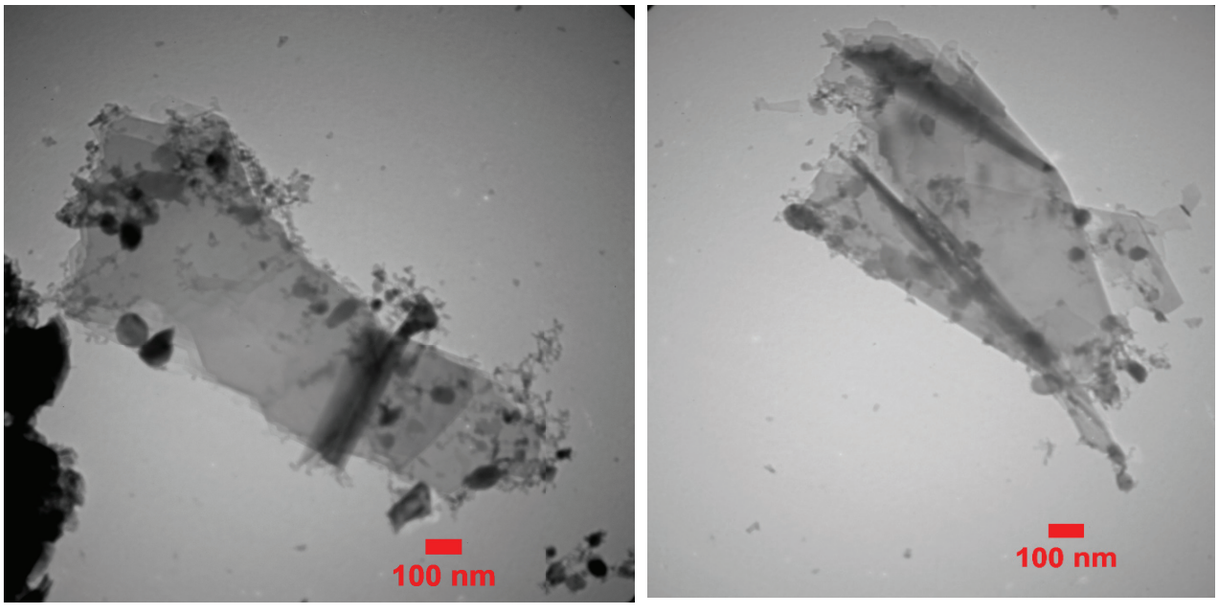

Fig. 6. TEM images of A PAMAM-GO nanocomposite.

3.3. The surface area of GO, AGO and A PAMAM-GO

Table 1 shows the results of the BET specific surface area and total pore volume as well as average pore size of absorbents. N_2 adsorption-desorption analyses showed that GO had the highest surface area and pore volume of 33 m^2/g and 0.14 cm^3/g respectively, being similar to the previous reported values [29]. Increasing in nitrate removal efficiency by chemical modification of adsorbents surface is related to: firstly, an enhancement in surface positive charges; and/or secondly, providing new surface functional groups having a higher affinity for nitrate [30–33]. Therefore, AGO and A PAMAM-GO with the small specific surface area had high absorption capacity, indicating that these absorbents had a good affinity for nitrate. Moreover, enhancement in surface positive charges of AGO and A PAMAM-GO has been improved by FT-IR analysis (Fig. 11).

Table 1
BET specific surface area, total pore volume and average pore size of absorbents

Adsorbent	S_{BET} (m^2/g)	Vp (cm^3/g)	L (nm)
GO	33	0.14	17.5
AGO	7.13	0.0083	46.66
A PAMAM-GO	8.76	0.0076	34.77

3.4. XRD pattern

Fig. 7 shows the XRD patterns of GO, AGO, PAMAMA-GO nanocomposite and A PAMAM-GO nanocomposite.

XRD patterns of graphite and graphene oxide have showed peaks at $2\theta = 26.49^o$, 37.3^o and 49.7^o [28,34,35].

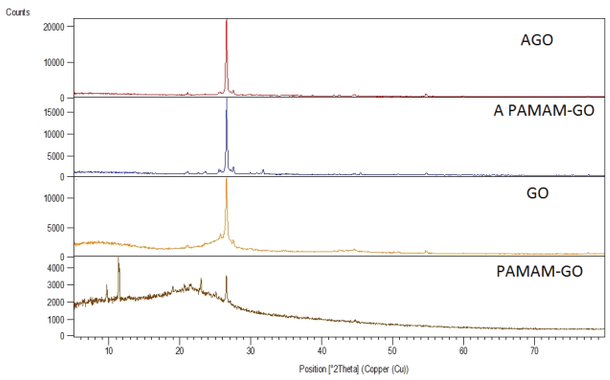

Fig. 7. XRD analysis of AGO, PAMAM-GO nanocomposite and A PAMAM-GO nanocomposite.

We observed the main peaks at 2θ = 14.93°, 26.56°, 27.52°, 54.68° for GO, at 2θ = 13.57°, 26.56°, 27.51° , 54.69° for AGO, at 2θ = 11.34°,11.44°, 26.55° for PAMAM-GO and at 2θ = 13.66°, 26.59°, 27.53° and 54.71 for A PAMAM-GO.

The pointed sharp peak reflects certain amount of crystallinity of AGO and A PAMAM-GO nanocomposite. In addition, diffraction peaks at 20 = 9.71, 11.34°, 11.44°, 18.99°, 20.63°, 21.53°, 22.98°, 25.06°, 26.55°, 34.76° indicated the semi crystalline nature of PAMAM-GO nanocomposite. After-composition of GO with PAMAM dendrimer, XRD pattern (Fig. 7) showed diffraction peak to be broader implied that the crystallinity was reduced. It increased again after activation process.

3.5. Thermal gravity analysis for the stability of A GO/PAMAMs nanocomposite (TGA studies)

As Fig. 8 shows, thermal stability of GO (not shown here), AGO and A PAMAM-GO nanocomposite have been studied by thermal gravity analysis. The results showed that stability of AGO and A PAMAM-GO nanocomposite was very good in comparison with GO. At a temperature of approximately 550°C, the thermal stability of AGO and A PAMAM-GO nanocomposite was found to decrease. GO has less thermal stability than AGO and A PAMAM-GO nanocomposite. Usually GO decomposition is started from 200°C [36,37].

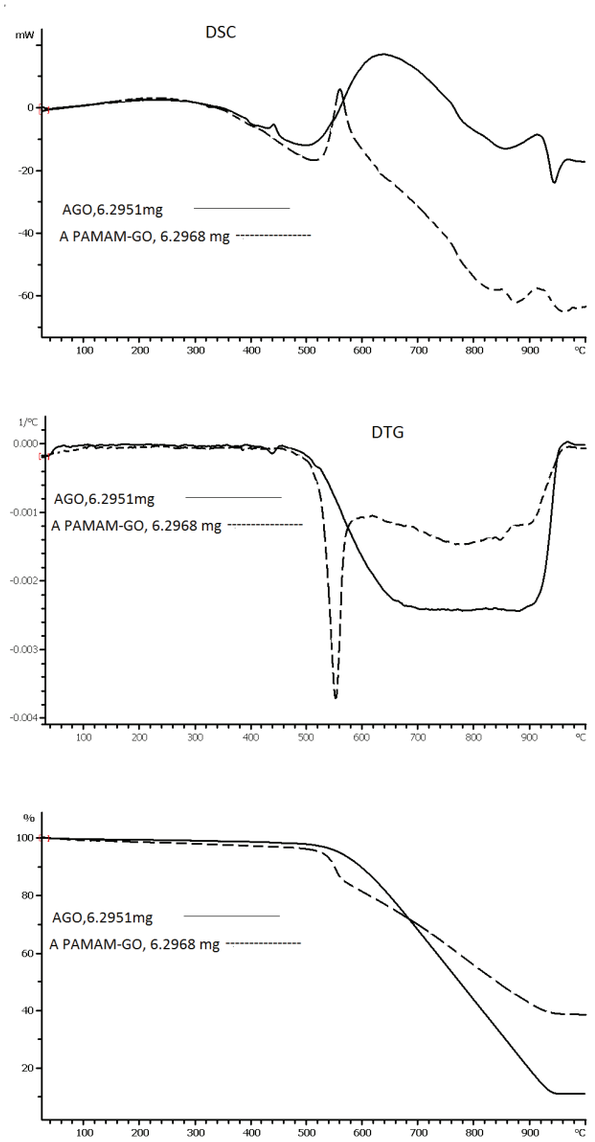

Fig. 8. Thermal stability analysis (TGA) of the AGO and A PAMAM-GO nanocomposite.

3.6. Examination of the chemical bonds of GO, AGO and A PAMAM-GO nanocomposite

FT-IR infrared spectroscopy tests were carried out to determine the chemical bonds in the samples of GO, AGO, A PAMAM-GO nanocomposite (Fig. 11). FTIR spectra of AGO and A PAMAM-GO samples differ from those of GO as evidenced by the intensity of the peaks in A PAMAM-GO and AGO. Comparing images clearly confirms intensity peaks in AGO and A PAMAM-GO.

IR analysis suggests that peaks 550–750 cm^{-1} and 1800 cm^{-1} indicate the presence of the C-Cl and H-Cl bonds respectively [38,39] and the peak in the region between 3100 and 3600 cm^{-1} indicates the presence of exchangeable protons, typically from alcohol, amine, amide or carboxylic acid groups. Additionally, the peak in the region between bending 1580 and 1650 cm^{-1} vibration indicates the presence of N-H bonds of secondary amine groups, which are favorable absorption for anions e.g. nitrate [30,40]. Moreover, oxygen atoms must be in the form of COOH/_OH and C =O groups with a peak of approximately 3400 cm^{-1} and 1700 ± 100 cm^{-1}, respectively [41]. So it seems characteristics band of quaternary ammonium groups have overlap by other bands [42].

In our study, FTIR analysis of GO, AGO and A PAMAM-GO samples showed that the peaks observed in 1638 cm^{-1} wavelengths (for AGO); 1622 cm^{-1} wavelengths (for A PAMAM-GO) have been related to both quaternary ammonium groups [42] and C = O [41] bonds. Moreover, the peaks observed in 2526.79 cm^{-1}, 2355.14 cm^{-1} wave-

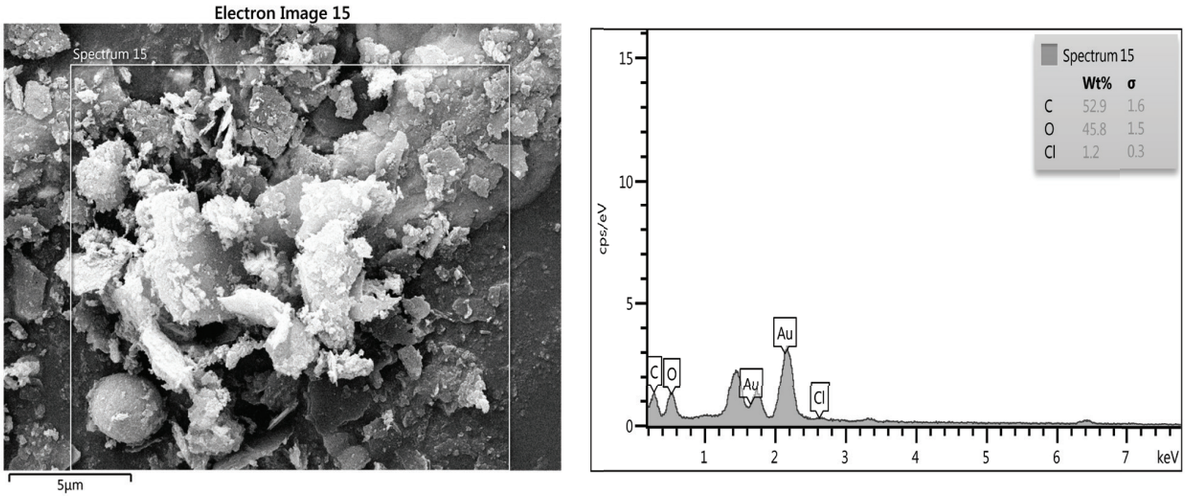

Fig. 9. EDS spectrum analysis of activated graphene oxide (AGO).

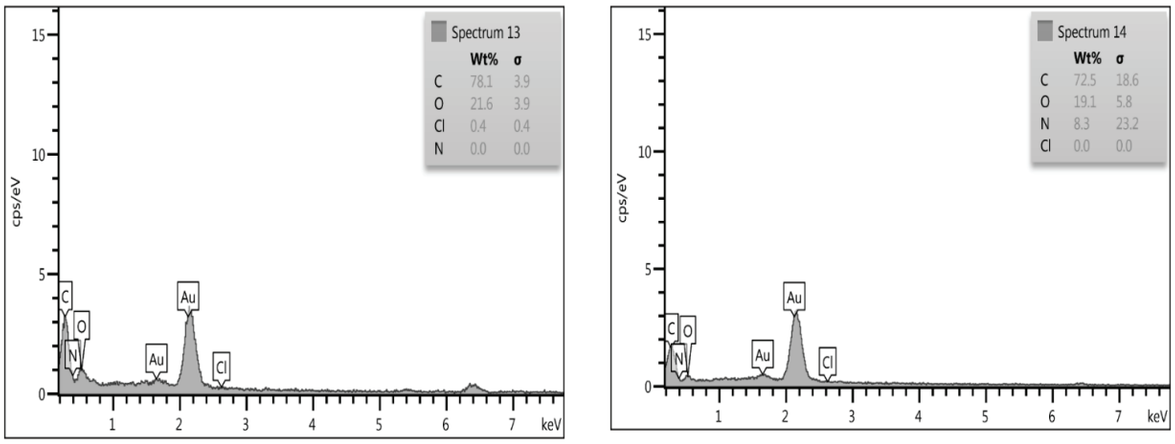

Fig. 10. EDS spectrum analysis of activated dendrimer-graphene oxide (A PAMAM-GO) nanocomposite.

lengths (for AGO) and 2342.97 cm^{-1}, 2362.19 cm^{-1}, 2358.85 cm^{-1}, 2356.04 cm^{-1} wavelengths (for A PAMAM-GO) have been related to quaternary ammonium groups [42].

In addition, FTIR analysis of GO, AGO and A PAMAM-GO samples showed that the peaks observed in 3452 cm^{-1} (for GO); 3425 cm^{-1} (for AGO); 3418 cm^{-1} (for A PAMAM-GO) wavelength were related to COOH/_OH bonds. The bands at around 1087 cm^{-1} (for AGO), 1088 cm^{-1} (for A PAMAM-GO), and 1048 cm^{-1} (for GO) are ascribed to the vibration of C–O; the bands at about 1622 cm^{-1} (for A PAMAM-GO) and 1638 cm^{-1} (for AGO), are ascribed to the vibration of C=C that could be assigned to the skeletal vibration of the original graphitic domain. These different functional groups on the surface of AGO and A PAMAM-GO indicate that large amount of oxygen-containing functional groups exist on AGO and A PAMAM-GO [28].

In addition, the peaks observed in 544.88 cm^{-1} and 603.92 cm^{-1} confirm the presence of chloride in the AGO sample and the peak observed in 1867 cm^{-1} confirms the presence of hydrochloric acid in the A PAMAM-GO. Functionalization of GO and PAMAM-GO by HCL and their activation are further confirmed with FT-IR coupled with EDS findings. Obvious changes are notable before and after GO and PAMAM composition and their activation.

Furthermore, A peak at around 1550 cm^{-1} in GO sample can be related to the existence of amine groups. It presents that why GO cannot serve as effective materials for nitrate removal from aquatic environment. However, after activation with HCl, this peak disappears significantly.

3.7. Effect of contact time on removal efficiency

As Fig. 12 shows, the effect of contact time was evaluated by varying the time in the range of 5–60 min while holding the other factors constant; (pH = 7.5 ± 0.2, Go and AGO concentration = 0.27 $g{\cdot}l^{-1}$, PAMAM concentration = 5$ml{\cdot}l^{-1}$, A PAMAM-GO & PAMAM-GO concentration = 0.025 $g{\cdot}l^{-1}$, nitrate concentration = 45 $mg{\cdot}l^{-1}$).

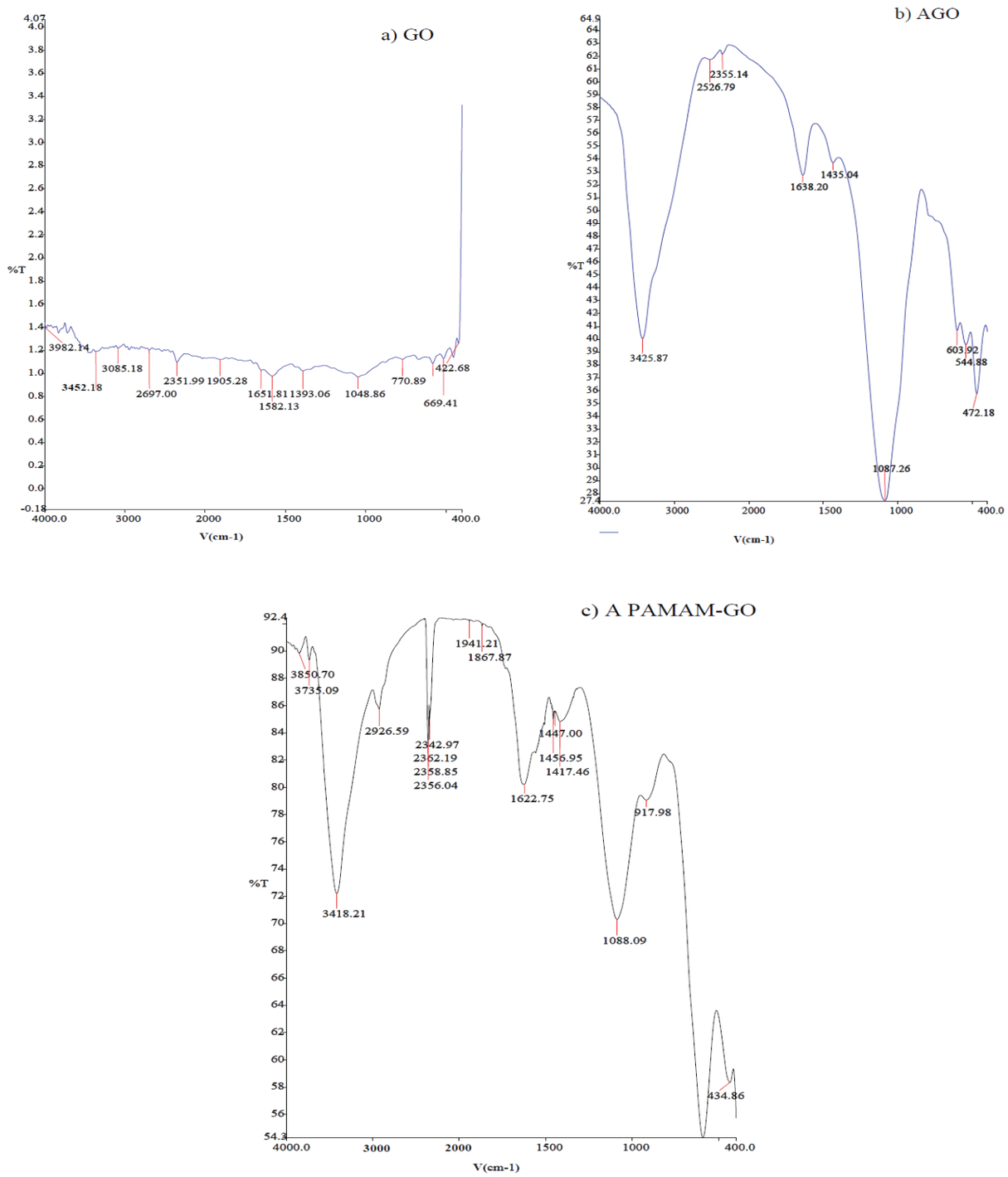

Fig. 11. FT-IR infrared spectroscopy tests; GO (a), AGO (b) and A PAMAM-GO nanocomposite (c).

These results show that removal efficiency is negative for PAMAM. PAMAM is a polyamidoamine compound and has N bonds, which may be formed to nitrate ions in the presence of oxygen molecules of water. In fact, PAMAM is a nitrogen source that can produce nitrate ions in the presence of water and oxygen.

One-way ANOVA showed a significant effect for contact time on the removal efficiency of nitrate by AGO and A PAMAM-GO ($p < 0.05$). Changing the contact time changed nitrate removal efficiency. Ait Haki et al. [43] and Wu et al. [44] reached same results in their study. With increase in contact time, the absorption of nitrate also increased;

it increased up to the optimal retention time (GO = 60 min; AGO = 40 min; A PAMAM-GO = 15 min; PAMAM & PAMAM-GO = 25 min) and decreased thereafter. It can be seen that NO_3 removal efficiency decreased as the contact time increased past 40 min for AGO, 60 min for GO, 25 min for PAMAM & PAMAM-GO and 15 min for A PAMAM- GO. Fig. 12 shows that optimum nitrate removal was 2% at 60 min for GO, 59.2% at 40 min for AGO, 1% at 25 min for PAMAM, 3.5% at 25 min for PAMAM-GO, and 86% at 15 min for A PAMAM-GO. The best and optimal nitrate removal efficiency was 90% in 15 min at 0.025 g/l A PAMAM-GO. Increasing the contact time to 25 min decreased removal efficiency to 82%; a further increase to 40 min increased efficiency to 94% for A PAMAM-GO. The increase in nitrate removal by A PAMAM-GO after 25 min and 55 min is related to changes in the nitrate concentration and ion exchange between the nitrate and chloride caused by activation with hydrochloric acid.

The presence of chloride ions on the surface of the A PAMAM-GO and AGO was confirmed by EDS and FT-IR analysis. As a result, ion exchange of nitrate with chloride occurs as:

$$(AGO + Cl^-) + NO_3^- \rightarrow (AGO + NO_3^-) + Cl^- \quad (3)$$

$$(A\ PAMAM\text{-}GO + Cl^-) + NO_3^- \rightarrow (A\ PAMAM\text{-}GO + NO_3^-) + Cl^- \quad (4)$$

In this regard, chloride ion concentration was 39.37 and 32.31 mg/l with a standard deviation of 5.7 and 3.2 for AGO and A PAMAM-GO, respectively, which is in the standard range according to a desirable maximum of 200 mg/l.

Monaco et al. also showed that 70% of emissions reduced within 30 min by a first-generation dendrimer [45].

3.8. Effect of pH on removal efficiency

The effect of pH on removal efficiency was evaluated by holding the other factors constant (GO and AGO concentration = 0.27 g l^{-1}, PAMAM & PAMAM-GO concentration = 5 mL/L, A PAMAM-GO concentration = 0.025 g/l, contact $time_{GO}$ = 60 min, contact $time_{AGO}$ = 40 min, contact $time_{A\ PAMAM\text{-}GO}$ = 15 min, contact $time_{PAMAM\ \&\ PAMAM\text{-}GO}$ = 25 min, nitrate concentration = 45 mg l^{-1}). The results of one-way ANOVA test show a significant difference for pH level ($p < 0.05$). Changes in pH altered removal efficiency by AGO and A PAMAM-GO; removal efficiency increased as pH increased to 7.5 and decreased from 7.5 to 9. Fig. 13 shows that nitrate removal efficiency for GO, AGO, PAMAM, PAMAM-GO and A PAMAM-GO was 1.1%, 55.4%, 3%, 6% and 70% at a pH of 4, respectively. This increased across the neutral range of pH so that the highest removal was obtained at a pH of 7.5 (2%, 59.2%, 1%, 3.5% and 86% for GO, AGO, PAMAM, PAMAM-GO and A PAMAM-GO respectively). Nitrate removal efficiency was considerably reduced at a pH of 9 (0%, 30%, 0.5%, 1% and 76% for GO, AGO, PAMAM, PAMAM-GO and A PAMAM-GO respectively).

The pH value plays an important role in the absorption of atomic ions by carbon-based nanomaterials by affecting the interaction between the sorbent and sorbing material. When the pH is higher than the pH_{PZC}, the negative charge on the surface causes electrostatic interactions attracting cationic species. When the pH is lower than pH_{PZC}, a

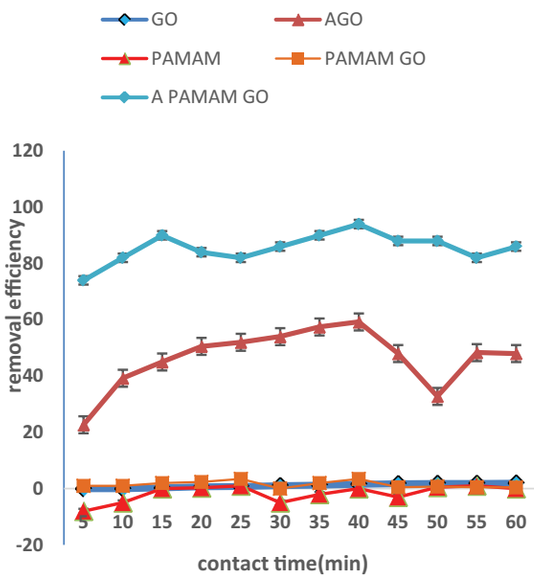

Fig. 12. Effect of contact time variations on the removal efficiency of nitrate (T = 23 ± 1°C, pH = 7.5 ± 0.2, GO & AGO concentration = 0.27 g l^{-1}, PAMAM & PAMAM-GO concentration = 5 ml l^{-1}, A PAMAM-GO concentration = 0.025 g l^{-1}, nitrate concentration = 45 mg l^{-1}).

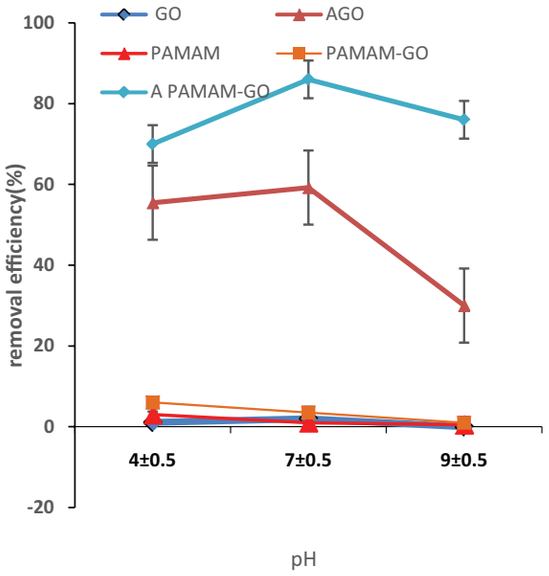

Fig. 13. Effect of pH variations on the removal efficiency of nitrate (T = 23 ± 1°C, GO & AGO concentration = 0.27 g l^{-1}, PAMAM & PAMAM-GO concentration = 5 mL/L, A PAMAM-GO concentration = 0.025 g/l, contact $time_{GO}$ = 60 min, contact $time_{AGO}$ = 40 min, contact $time_{A\ PAMAM\text{-}GO}$ = 15 min, contact time $_{PAMAM\ \&\ PAMAM\text{-}GO}$ = 25 min, nitrate concentration = 45 mg l^{-1}).

positive charge is created on the surface of nanomaterials sorbing anionic species. In other words, the positive surface charge of the sorbent increases absorbance of anions, and an electro-static attraction develops.

It can be concluded that nitrate with a negative charge is well removed in these conditions [11,46,47].

It seems that there have been most electrostatic interactions between positive sites of sorbent and nitrate ion. However, electrostatic interactions are not effective factors alone, and it is one of the factors that can contribute to this field. If the electrostatic forces are effective alone, removal rate should be higher at pH = 4 ± 0.5, which absorbent charge is more positive, while absorbent surface removal rate has increased at pH = 7.5 that there is a little negative charge. Functional groups on the surface of sorbent and competition between nitrate and other anions are some of these factors.

Therefore, according to the results of the EDAX analysis and functional groups on the surface of AGO, the reaction of nitrate removal can be as:

$$AGO\text{-}H_2O + NO_3^- \rightarrow AGO - NO_3^- + H_2O \quad (5)$$

And at high pH as:

$$AGO\text{-}OH^- + NO_3^- \rightarrow AGO - NO_3^- + H_2O \quad (6)$$

In addition, the reaction of nitrate removal by A PAMAM-GO can be as:

$$A\ PAMAM\text{-}GO\text{-}H_2O + NO_3^- \rightarrow A\ PAMAM\text{-}GO\text{-}\ NO_3^- + H_2O \quad (7)$$

And at high pH as:

$$A\ PAMAM\text{-}GO\text{-}OH^- + NO_3^- \rightarrow A\ PAMAM\text{-}GO\text{-}\ NO_3^- + H_2O \quad (8)$$

In that case, defects and decrease in absorption at high pH can be explained.

As mentioned earlier, efficiency of nitrate removal at pH = 9 was reduced from 86% to 78% in the duration of 15 min.

It should be noted that in the solution with pH = 9, another anion e.g. chloride may be presented with high concentrations. Therefore, the competition between the other anion(s) and nitrate for absorption can also be effective in reducing the absorption rate.

In addition, the main reason for decrease in absorption at high levels of pH is the ionization between the sorbent and sorbate creating a repulsive forces and decreasing absorption [48]. Increasing the pH of solution increased the nitrate concentration and separation of the functional groups [49]. The solubility of the nitrate also increased at high pH value, therefore decreasing in the absorption is possible [50].

The results were in agreement with those of similar research studies. Zheng et al. reported that increasing the pH to above 8 decreased arsenate removal efficiency using GO-Fe sorbent [51]. Lead ion absorption onto GO decreased the absorption rate when the pH value dropped to less than 6. According to Huang et al., maximum absorption of lead ions occurs at a neutral range of pH [52].

Eslami et al. achieved the highest removal efficiency at a pH of 8 for removal of chlorophenol from an aquatic environment using GO [50].

3.9 Effect of GO, AGO, PAMAM, PAMAM-GO and A PAMAM-GO concentration

The effect of the concentration of GO, AGO (0.27, 0.4, 0.75, and 1 g/l) PAMAM, PAMAM-GO (3, 5 and 10 mL/L) and A PAMAM-GO (0.008, 0.017, 0.025 and 0.033 g/l) on performance was investigated while holding the other factors constant (T = 23 ± 1°C, $pH_{PAMAM\text{-}GO\&PAMAM}$ = 4± 0.5, pH_{others} = 7.5 ± 0.2, contact $time_{GO}$ = 60 min, contact $time_{AGO}$ = 40 min, contact $time_{A\ PAMAM\text{-}GO}$ = 15 min, contact $time_{PAMAM\text{-}GO}$ = 25 min, nitrate concentration = 45 mg l^{-1}). One-way ANOVA test showed a significant effect for AGO and A PAMAM-GO concentration for nitrate removal ($p < 0.05$). This means that an increase in concentration increased nitrate removal efficiency.

Fig. 14 shows that the nitrate removal efficiency increased as the GO, AGO and A PAMAM-GO concentrations increased. The optimum concentration was 0.025 g/l for A PAMAM-GO and 0.4 g/l for AGO; the removal concentration decreased above and below this value. The reasons for the increase in efficiency of A PAMAM-GO and AGO is likely related to an increase in the active surface sites, increasing contact of the nitrate with A PAMAM-GO and AGO, and the redox reactions. It is important to note that increasing the GO and AGO concentrations from 0.4 to 1 g/l, A PAMAM-GO concentration from 0.025 to 0.0033 g/l and the PAMAM and A PAMAM-GO concentration from 5 to 10 mL/L decreased nitrate removal efficiency. This indicates that excess ions from the GO, AGO, PAMAM, AMAM-GO or A PAMAM-GO can cause turbidity in the treated solution and interference in the treatment, reducing its effectiveness.

The concentration of 0.025 g/l of A PAMAM-GO (for a 45 mg/l nitrate concentration) was highly efficient due to its large effective area.

The minimum required sorbent in previous studies has been 1 g/l (for 5 mg/l nitrate concentration). Similar studies using GO found that only 7% of the nitrate (with 5 mg/l concentration) was removed after 48 h. They also showed that 1 g/l of nZVI-GO (GO coated with iron nanoparticles) removed 82% of the nitrate (with 5 mg/l concentration) after about 2.5 h [19].

3.9..1 Effect of nitrate concentration

Fig. 15 shows the effect of initial nitrate concentration. Maximum nitrate removal efficiency of about 90% was achieved using 0.025 g A PAMAM-GO at an initial concentration of 45 mg/l of nitrate. This was 80%, 4.5%, 3%, and 3.5% for 0.4 g AGO, 1 g GO, 5 mL PAMAM and 5 mL PAMAM-GO, respectively. Removal efficiency decreased as the nitrate concentration increased from 45 to 110 mg/l. Removal efficiency of 110 mg/l nitrate was 60% for A PAMAM-GO, 55% for AGO, 0% for PAMAM, 0% for PAMAM-GO and 0.2% for GO. These results are in agreement with those of other studies. A decrease in nitrate removal has been reported due to lack of sufficient active

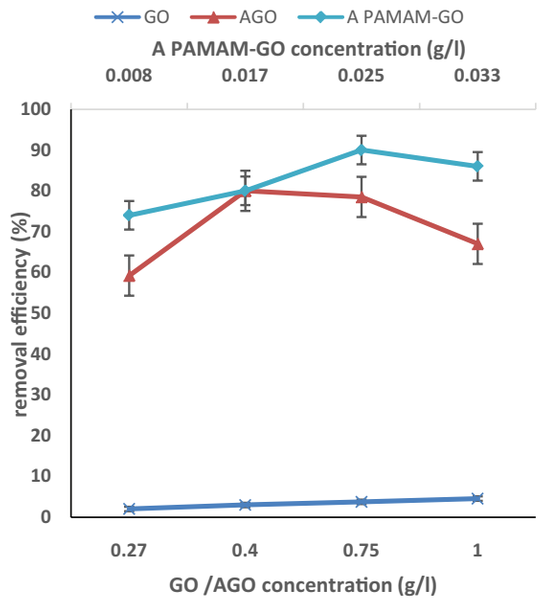

Fig. 14. Effect of GO, AGO, PAMAM-GO & A PAMAM-GO concentration variations on the removal efficiency of nitrate (T = 23 ± 1°C, $pH_{PAMAM-GO\&PAMAM}$ = 4 ± 0.5, pH_{others} = 7.5 ± 0.2, contact $time_{GO}$ = 60 min, contact $time_{AGO}$ = 40 min, contact $time_{A\ PAMAM-GO}$ = 15 min, contact $time_{PAMAM-GO}$ = 25 min, nitrate concentration = 45 mg l^{-1}).

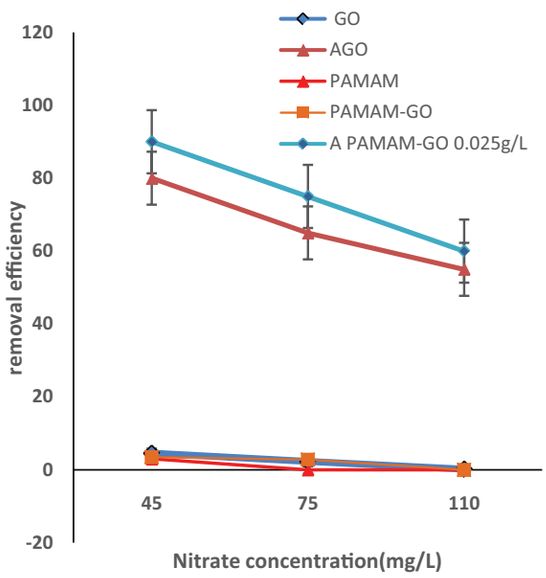

Fig. 15. Effect of nitrate concentration variations on the removal efficiency of nitrate (T = 23 ± 1°C, $pH_{PAMAM-GO\&PAMAM}$ = 4 ± 0.5, pH_{others} = 7.5 ± 0.2, contact $time_{GO}$ = 60 min, contact $time_{AGO}$ = 40 min, contact $time_{A\ PAMAM-GO}$ = 15 min, contact $time_{PAMAM-GO}$ = 25 min, GO = 1 g/l, AGO = 0.4 g/l).

sites for high concentrations of nitrates [3]; the sorption capacity decreases as the concentration increases [53].

3.9.2. Absorption isotherms of AGO and A PAMAM-GO

Determination of sorption isotherms and sorbent capacity are the most important characteristics considered in studies of the absorption of pollutants onto different sorbents. In this study, equilibrium sorption was modelled using the Langmuir, Freundlich, Elovich and Temkin models. Fig. 9 and Table 1 present summary results of these studies.

Langmuir isotherm

The homogeneous monolayer coverage governs the Langmuir isotherm model [20] with equivalency of the sites.

The linear form of the Langmuir model can be expressed as:

$$\frac{1}{q_e} = \frac{1}{abC_e} + \frac{1}{b} \tag{9}$$

where q_e is the amount of ions adsorbed at equilibrium time (mg/g), b is the maximum absorption capacity and a is the Langmuir constant related to the sites and energy of sorption [54]. A straight line curve with a slope of $1/ab$ and intercept of $1/b$ will be achieved by plotting $1/q_e$ against $1/C_e$. Sorption equilibrium constant K_L (l/g) depends on the value of a and b and is calculated as $K_L = a \times b$. The main parameter of the Langmuir isotherm is a constant dimensionless parameter called the equilibrium parameter (R_L) that is determined as:

$$R_L = \frac{1}{1 + K_L C_0} \tag{10}$$

The desirability of sorption in the Langmuir model can be specified using the R_L dimensionless factor. $R_L > 1$ denotes negative sorption, $R_L = 1$ denotes linear sorption, $R_L = 0$ denotes irreversible sorption, and $0 < R_L < 1$ denotes optimal sorption [46,52,54,55].

Freundlich isotherm

The linear form of the Freundlich equation can be expressed as:

$$\log q_e = \log K_f + \frac{1}{n}(\log C_e) \tag{11}$$

where q_e is equilibrium sorption capacity (mg/l), C_e is equilibrium concentration of the sorbing material (mg/l), and k and n are the Freundlich constants obtained from plotting (on the Y axis) against , making the slope $1/n$ and the intercept log k_f [46,52,54,55]. It is assumed that heterogeneous surface with different energy sites is available for absorption in Freundlich model. In general, absorption capacity increases by increasing value. Additionally, values of n in Freundlich isotherm model is a measure of the absorption rate. If the n is less than *1* indicates a weak absorption, n between *2* and *1* represents the average absorption and n between *2* to *10* represents optimal absorption. Furthermore, n represents the distribution of absorbate particles to the absorbent surfaces so that *1/n* with values *0* and *1* indicates the heterogeneity of the surface. The heterogeneity of surface increases when it closes to zero. If it is less

than one, it would indicate absorption Freundlich isotherm [46,52,54,55].

Temkin isotherm

It is assumed that the drop in heat absorption is linear in the Temkin model as:

$$q_e = B\ ln\ A_T + B\ Ln\ C_e \quad (12)$$

where q_e is the amount of adsorbate adsorbed at equilibrium (mg/g); C_e is concentration of adsorbate in solution at equilibrium (mg/L). B is a constant related to the heat of absorption, and it is defined by the expression $B = RT/b_T$, b_T is the Temkin constant (J/mol), T is the absolute temperature (K), R is the gas constant (8.314 J/mol K), and A_T is the Temkin isotherm constant (L/g) from the plot of q_e vs. Ln C_e, B and A_T can be calculated from the slopes (B) and intercepts ($B\ \ln A_T$) respectively [56].

Elovich isotherm

The Elovich equation [13] is expressed as:

$$Ln\left(\frac{q_e}{c_e}\right) = \ln\left(K_E q_m\right) - \frac{q_e}{q_m}$$

where K_E and q_m represent the equilibrium constant and the Elovichsorption capacity, respectively. The slope and intercept of the Ln (q_e/c_e) versus q_e give the parameters [13].

Table 1 and Fig. 16 present the summary results of these studies.

The correlation coefficient (R^2) for nitrate sorption onto AGO and A PAMAM-GO for Freundlich models

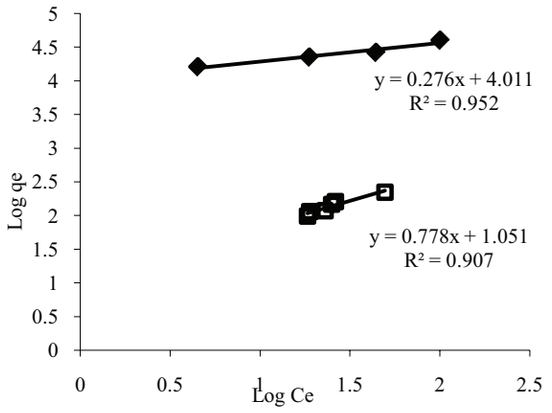

b)Freundlich isotherm plot for AGO and A PAMAM-GO

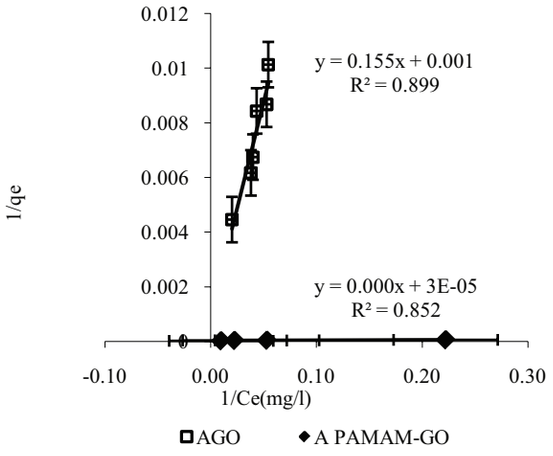

a)Langmuir isotherm plot for AGO and A PAMAM-GO

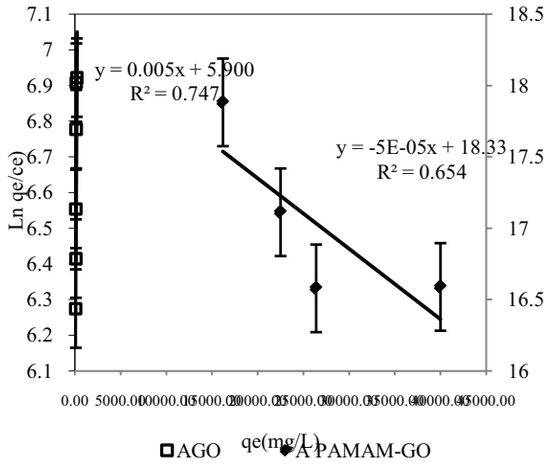

d) Elovich isotherm plot for AGO and A PAMAM-GO

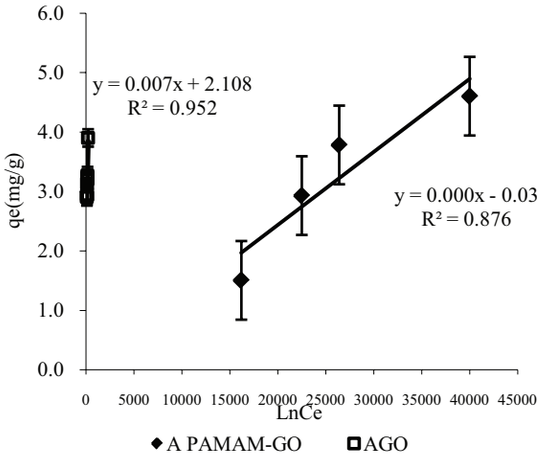

c) Temkin isotherm plot for AGO and A PAMAM-GO

Fig. 16. Langmuir, Freundlich, Elovich and Temkin models plot for AGO and A PAMAM-GO sorption.

Table 2
Parameters of Langmuir and Freundlich isotherm models for nitrate removal on AGO and A PAMAM-GO nanocomposite for nitrate removal on AGO and A PAMAM-GO nanocomposite

Langmuir					Freundlich				Model
R_L	K_L	R^2	a	b	R^2	$1/n$	K_f	n	Parameter
0.003	6.42	0.8998	0.00642	1000	0.9073	0.7784	11.26	1.2846	AGO
2.22	9999.9	0.8529	0.466	3333.33	0.9523	0.2767	1025.88	3.6140	A PAMAM-GO

Table 3
Maximum sorption capacity comparison with some similar sorbents of nitrate

No.	Adsorbent	Amount adsorbed	Concentration range	Contact time	Temperature	Adsorbent dose	Reference
1	Powdered activated carbon	10 mmol/g	–	60 min	25C		[29]
2	Carbon nanotubes	25 mmol/g	–	60 min	25C		[58]
3	$ZnCl_2$ treated coconut granule activated carbon	10.2 mg/g	5–200 mg/L	2 h	25C		[14]
5	Chitosan coated zeolite	0.6–0.74 mmol/g	10–3100 mg/L	72 h	4 C and 20C	.4 g/200 ml	[5]
6	Chitosan hydrobeads	92.1 mg/g	1–1000 mg/L	1440 min	30C	1 g/50 ml	[5]
7	Conditioned cross-linked chitosan beads	104.0 mg/g	25–1000 mg/L	24 h	30C		[11]
8	Sugarcane bagasse	1.41 mmol/g	1–30 mg/L	48 h	30C	.1 g/50 ml	[47]
9	Original and activated redmud	1.859 and 5.858 mmol/g	5–250 mg/l	60 min	Room temperature		[59]
10	Cross-linked and quaternized chinese reed	7.55 mg/g	10–40 mg/dm^3	10 min	25C	.2 g/50 ml (0–1 g)	[5]
11	Pure alkaline lignin	1.8 mmol/g	1–30 mg/l	48 h	30C	.1 g/50 ml	[47]
12	Sepiolite activated by HCl	38.16 mg/g	100 mg/l	5 min	–		[13]
13	Chemically modified sugar beet bagasse	9.14–27.55 mg/g	10–200 mg/L	–	25C - 45 C	.1 g/50 ml	[60]
	Unmodified sepiolite	408 mmol/kg	–	–	–		[11]
14	Surfactant-modified sepiolite	453 mmol/kg	–	–	–		[11]
15	Ammonium-functionalized mesostructured silica	46.0 mg/g	100–700 mg/L	60min	5C	5 g/l–(1–10 g/l)	[59]
16	Carbon nanotubes	25 mmol/g	–	60 min	25C		[58]
17	Nano-Alomina	4 mg/g	1–100 mg/l	24 h	25 C	1 g/l	[5]
18	AGO	1000 mg/g	45–110 mg/l	40 min	ROOM temperature	0.27 g/L	This study
19	A PAMAM-GO nanocomposite	1025.88 mg/g	45–200 mg/l	15 min	ROOM temperature	0.025 g/l	This study

were 0.9073 and 0.9523, respectively. The results show that Freundlich model has been fairly fitted with nitrate sorption data.

Since values of obtained n in nitrate sorption by AGO and A PAMAM-GO nanocomposite were 1.2846 and 3.6140, respectively, the Freundlich isotherm model is optimal for A PAMAM-GO and average for AGO.

In this study, $1/n$ were 0.7784 and 0.2767 for AGO and A PAMAM-, respectively, therefore we can mention that the absorbent surface is extremely in heterogeneous mode. This is also confirmed by FE-SEM images. The values obtained from the Langmuir isotherm indicate that this isotherm is not an appropriate model [57] for AGO or A PAMAM-GO. The maximum absorption capacity of 1025.88 mg/g was obtained with A PAMAM-GO nanocomposite that is much higher than the amounts reported by other studies.

In this study, the Freundlich model was selected as the most appropriate model.

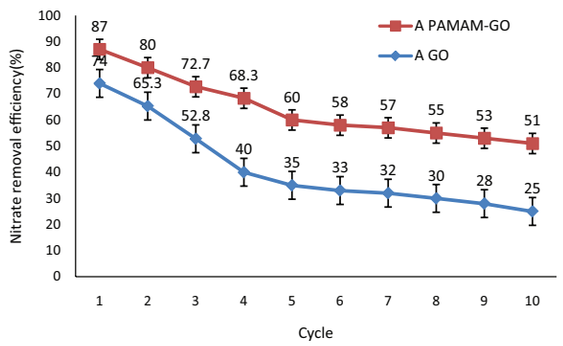

Fig. 17. Effect of regeneration.

The value in this study shows that A PAMAM-GO nanocomposite is more effective than other absorbents used for nitrate removal until now (Table 1).

3.9.3. Regeneration

After nitrate removal process, regeneration study of AGO and A GO/PAMAMs nanocomposite was performed with 0.1 M NaCl solution and 5–60 min contact time. The optimum contact time for regeneration of A PAMAM-GO and AGO was 20 min and 50 min, respectively. This regeneration mechanism is based on ion exchange reaction. As Fig. 17 shows, nitrate removal in the first cycle has only 3% decreases for A PAMAM-GO, while it was 6% for GO. In the fifth cycle, it decreases up to 30% and 45% for A PAMAM-GO and AGO, respectively. It seems that A PAMAM-GO has higher efficiency in regeneration than AGO.

3.10. Sorption mechanism of nitrate ion on AGO and A GO/PAMAMs nanocomposite

FTIR analyses show that the main mechanism of nitrate ion removal by AGO and A GO/PAMAMs nanocomposite is the ion exchange between nitrate and chloride ions. The reports of Chauhan et al. and Banu et al. approved these results [61]. In addition, Mohan et al., Banu et al. and Wu et al. reported that hydrogen bonding with π system of nitrate and hydroxyl groups was possible (NO_3^-··· HO) [44,61,62].

4. Conclusion

Nanotechnology has attracted considerable attention for removal of environmental pollutants. The present study tested nitrate removal by GO, AGO, PAMAM, PAMAM-GO and A PAMAM-GO for the first time in the world by examining the effects of pH, contact time, nitrate concentration, and the concentration of GO, AGO, PAMAM, PAMAM-GO and APAMAM-GO on nitrate removal. GO is a new nanostructure of carbon nanomaterials that was not capable of removing nitrate alone. PAMAM is also considered today in many biomedical and environmental areas, but the results of this study showed that it was not capable of removing nitrate. In this study, we have developed GO and PAMAM efficiency by activating and composing them. Therefore, it led to increase the removal efficiency in the AGO and A PAMAM-GO, as the results showed that 0.4 g/l AGO could remove 80% of the nitrate in 40 min at a pH of 7.5. The highest removal efficiency was obtained with A PAMAM-GO (90% at 0.025 g/l A PAMAM-GO, pH of 7.5, 15 min contact time). We also investigated the mechanism involved in the enhancement. By some characterizations using EDS and FTIR, we found that the ion exchange between nitrate and chloride was the main mechanism of nitrate removal by AGO and A PAMAM-GO according to the functionalized A PAMAM-GO and AGO using hydrochloric acid.

The literature review clarified that the minimum effective time and minimum amount of required sorbent for nitrate removal were at least 1 h and 1 g/l, respectively. Thus, it can be concluded that the AGO and A PAMAM-GO have more functionality for nitrate removal from aqueous solutions.

Acknowledgements

This article is extracted from Ph.D. thesis supported by the National Elites Foundation and Zanjan Water & Wastewater Company that is implemented in the faculty of Civil, Water and Environmental Engineering of Shahid Beheshti University.

Abbreviations

G	—	Graphene
GO	—	Graphene Oxide
AGO	—	Activated GO
PAMAM	—	Polyamidoamine;
PAMAM-GO	—	Dendrimer-graphene oxide nanocomposite
A PAMAM-GO	—	Activated PAMAM-GO nanocomposite
PAMAM-G_2	—	The second generation of Polyamide amine dendrimer
FE-SEM	—	Field-emission scanning electron microscope
EDS	—	Energy-dispersive X-ray spectroscopy
FTIR	—	Fourier Transform Infrared Spectroscopy.

References

[1] Nitrate and Nitrite in Drinking-Water, in, World Health Organization WHO Press,Geneva, Switzerland, 2011.
[2] N. Bryan, J. Loscalzo, eds, Nitrite and nitrate in human health and disease in, New York, NY, Springer, Humana Press., 2011.
[3] I. Mahamudur, Development of adsorption media for removal of lead and nitrate from water, in, Thesis to PhD degree of philosophy in chemistry. Department of chemistry national institute of technology Rourkela, India, 2008, pp. 118–156.
[4] S. Archna, K. Sharma, R.C. Sobti, Nitrate removal from ground water: a review, E-J CHEM, 9 (2012) 1667–1675.
[5] S.C. Ahn, S.-Y. Oh, D.K. Cha, Enhanced reduction of nitrate by zero-valent iron at elevated temperatures, J. Hazard. Mater., 156 (2008) 17–22.
[6] V. Polshettiwar, S. Rajender, Varma, Green chemistry by nano-catalysis, Green Chem., 12 (2012) 743–754.
[7] F. Guo, G. Silverberg, S. Bowers, S.-P. Kim, D. Datta, V. Shenoy, R.H. Hurt, Graphene-based environmental barriers, Environ. Sci. Technol., 46 (2012) 7717–7724.

[8] A.K. Geim, Graphene: status and prospects, Science, 324 (2009) 1530–1534.
[9] C.N. Rao, R. Sood, A.K. Subrahmanyam, A. Govindaraj, Graphene: the new two-dimensional nanomaterial, Angew. Chem., Int. Ed, 48 (2009) 7752–7777.
[10] S.S. Gupta, T.S. Sreeprasad, S.M. Maliyekkal, S.K. Das, T. Pradeep, Graphene from Sugar and its application in water purification, ACS Appl. Mater. Interfaces, 4 (2012) 4156–4163.
[11] E. Eroglu, W. Zang, P.K. Eggers, X. Chen, R.A. Boulos, M.H. Wahid, S.M. Smith, C.L. Raston, Nitrate uptake by p-phosphonic acid calix[8]arene stabilized graphene, Chem. Commun., 49 (2013) 8172–8174.
[12] W. Liu, Catalyst technology development from macro-micro-down to nano-scale, China Particuology, 3 (2005) 383–394.
[13] S.K. Kumar, S.S. Kakan, N. Rajesh, A novel amine impregnated graphene oxide adsorbent for the removal of hexavalent chromium, Chem. Eng. J, 230 (2013) 328–337.
[14] X.-j. Hu, Y.-g. Liu, H. Wang, A.-w. Chen, G.-m. Zeng, S.-m. Liu, Y.-m. Guo, X. Hu, T.-t. Li, Y.-q. Wang, L. Zhou, S.-h. Liu, Removal of Cu(II) ions from aqueous solution using sulfonated magnetic graphene oxide composite, Sep. Purif. Technol., 108 (2013) 189–195.
[15] H. Wang, X.-Z. Yuan, Y. Wu, H. Huang, G. Zeng, Y. Liu, X. Wang, N. Lin, Y. Qi, Adsorption characteristics and behaviors of graphene oxide for Zn(II) removal from aqueous solution, Appl. Surface Sci., 279 (2013) 432–440.
[16] H. Wang, X.-Z. Yuan, Y. Wu, H. Huang, X. Peng, G. Zeng, H. Zhong, J. Liang, M. Ren, Graphene-based materials: Fabrication, characterization and application for the decontamination of wastewater and wastegas and hydrogen storage/generation, Adv. Colloid Interface Sci., 195–196 (2013) 19–40.
[17] H. Wang, X.-Z. Yuan, New generation material for oilspill cleanup, Environ. Sci. Pollut. Res., 21 (2014) 1248–1250.
[18] H. Wang, X. Yuan, G. Zeng, Y. Wu, Y. Liu, Q. Jiang, S. Gu, Three dimensional graphene based materials: Synthesis and applications from energy storage and conversion to electrochemical sensor and environmental remediation, Adv. Colloid Interf. Sci., 221 (2015) 41–59.
[19] E. Motamedi, M.T. Atouei, M.Z. Kassaee, Comparison of nitrate removal from water via graphene oxide coated Fe, Ni and Co nanoparticles, Mater. Res. Bull, 54 (2014) 34–40.
[20] B. Hayati, N. Mahmoodi, A. Maleki, Dendrimer-titania nanocomposite: synthesis and dye-removal capacity, Res. Chem. Intermed., (2013) 1–15.
[21] M. Sadeghi-Kiakhani, M. Arami, K. Gharanjig, Dye removal from colored-textile wastewater using chitosan-PPI dendrimer hybrid as a biopolymer: Optimization, kinetic, and isotherm studies, J. Appl. Polym. Sci., 127 (2013) 2607–2619.
[22] P.K. Maiti, T. Çağın, G. Wang, W.A. Goddard, Structure of PAMAM dendrimers: Generations 1 through 11, Macromolecules, 37 (2004) 6236–6254.
[23] P. Ilaiyaraja, A.K. Singha Deb, D. Ponraju, B. Venkatraman, Removal of cobalt from aqueous solution using xanthate functionalized dendrimer, Desal. Water Treat., 52 (2014) 438–445.
[24] T. Zhou, F. Chen, K. Liu, H. Deng, Q. Zhang, J. Feng, Q. Fu, A simple and efficient method to prepare graphene by reduction of graphite oxide with sodium hydrosulfite, Nanotechnology, 22 (2011) 045704.
[25] W.S. Hummers, R.E. Offeman, Preparation of graphitic oxide, J. Am. Chem. Soc., 80 (1958) 1339–1339.
[26] R. Esfand, D.A. Tomalia, Laboratory synthesis of poly(amidoamine)(PAMAM) dendrimers, in: Dendrimers and Other Dendritic Polymers, John Wiley & Sons, Ltd, 2002, pp. 587–604.
[27] APHA, WPCF, Standard method for the examination of water and wastewater, 21th ed., Washingon D.C, 2005.
[28] G. Zhao, J. Li, X. Ren, C. Chen, X. Wang, Few-layered graphene oxide nanosheets as superior sorbents for heavy metal ion pollution management, Environ. Sci. Technol., 45 (2011) 10454–10462.
[29] A. Khani, M. Mirzaei, Comparative study of nitrate removal from aqueous solution using powder activated carbon and carbon nanotubes, in: 2nd International IUPAC Conference on Green Chemistry, Russia, 2008, pp. 14–19.
[30] P. Loganathan, S. Vigneswaran, J. Kandasamy, Enhanced removal of nitrate from water using surface modification of adsorbents – A review, J. Environ. Manage., 131 (2013) 363–374.
[31] J.-Y. Lee, S.-J. Seo, S.-H. Yun, S.-H. Moon, Preparation of ion exchanger layered electrodes for advanced membrane capacitive deionization (MCDI), Water Res., 45 (2011) 5375–5380.
[32] P.M. Biesheuvel, R. Zhao, S. Porada, A. van der Wal, Theory of membrane capacitive deionization including the effect of the electrode pore space, J. Colloid Inter. Sci., 360 (2011) 239–248.
[33] Y.-J. Kim, J.-H. Choi, Selective removal of nitrate ion using a novel composite carbon electrode in capacitive deionization, Water Res, 46 (2012) 6033–6039.
[34] P. Ramesh, S. Bhagyalakshmi, S. Sampath, Preparation and physicochemical and electrochemical characterization of exfoliated graphite oxide, J. Colloid Inter. Sci., 274 (2004) 95–102.
[35] A.S.K. Kumar, N. Rajesh, Exploring the interesting interaction between graphene oxide, Aliquat-336 (a room temperature ionic liquid) and chromium(vi) for wastewater treatment, RSC Adv., 3 (2013) 2697–2709.
[36] F. Najafi, M. Rajabi, Thermal gravity analysis for the study of stability of graphene oxide–glycine nanocomposites, Int. Nano Lett., 5 (2015) 187–190.
[37] U. Rana, S. Malik, Graphene oxide/polyaniline nanostructures: transformation of 2D sheet to 1D nanotube and in situ reduction, Chem. Commun., 48 (2012) 10862–10864.
[38] L. Kimmel, M. Coelhan, W. Vetter, H. Parlar, FTIR spectroscopic characterization of chlorinated camphenes and bornenes in technical toxaphene, Environ. Sci. Technol., 34 (2000) 3041–3045.
[39] M.B. Blanco, I. Bejan, I. Barnes, P. Wiesen, M.A. Teruel, FTIR product distribution study of the Cl and OH initiated degradation of methyl acrylate at atmospheric pressure, Environ. Sci. Technol., 44 (2010) 7031–7036.
[40] T.N. Pliev, A.E. Mysak, The analysis of polyethylenepolyamines by NMR and infrared spectroscopy, J. Appl. Spectrosc., 19 (1973) 1620–1625.
[41] S.-T. Yang, S. Chen, Y. Chang, A. Cao, Y. Liu, H. Wanga, Removal of methylene blue from aqueous solution by graphene oxide, J. Colloid Interf. Sci., 359 (2011) 24–29.
[42] A. Keränen, T. Leiviskä, B.-Y. Gao, O. Hormi, J. Tanskanen, Preparation of novel anion exchangers from pine sawdust and bark, spruce bark, birch bark and peat for the removal of nitrate, Chem. Eng. Sci., 98 (2013) 59–68.
[43] M. Ait Haki, M. Laabd, H. Chafai, H. Kabli, M. Ez-zahery, M. Bazzaoui, R. Lakhmiri, A. Albourine, Comparative adsorption of nitrate ions on the polypyrrole and polyaniline from aqueous solution, J. Dispersion Sci. Technol., 38 (2017) 598–603.
[44] Y. Wu, Y. Wang, J. Wang, S. Xu, L. Yu, C. Philippe, T. Wintgens, Nitrate removal from water by new polymeric adsorbent modified with amino and quaternary ammonium groups: Batch and column adsorption study, J. Taiwan Inst. Chem. Eng., 66 (2016) 191–199.
[45] O.N. Monaco, S.C. Tomas, M.K. Kirrane, A.M. Balija, Bis(benzylamine) monomers: One-pot preparation and application in dendrimer scaffolds for removing pyrene from aqueous environments, Beilstein J. Org. Chem., 9 (2013) 2320–2327.
[46] L. Sun, H. Yu, B. Fugetsu, Graphene oxide adsorption enhanced by in situ reduction with sodium hydrosulfite to remove acridine orange from aqueous solution, J. Hazard. Mater., 203–204 (2012) 101–110.
[47] A. Eslami, A.R. Yazdanbakhsh, A. Asadi, M. Ghadimi, Nitrate removal from drinking water using modified natural clays, J. Water Wastewater, 25 (2014) 127–134.
[48] J. Fanning, The chemical reduction of nitrate in aqueous solution, Coord. Chem. Rev., 199 (2000) 159–179.
[49] M. Islam, R. Patel, Physicochemical characterization and adsorption behavior of Ca/Al chloride hydrotalcite-like compound towards removal of nitrate, J. Hazard. Mater., 190 (2011) 659–668.
[50] A. Eslami, A.R. Yazdabakhsh, H. Daraee, F.S. Karimi, Removal of 4-chlorophenol from aqueous solutions using graphene oxide nanoporous adsorbent, J. Water Wastewater, 26 (2015) 19–26.

[51] K. Zhang, V. Dwivedi, C. Chi, J. Wu, Graphene oxide/ferric hydroxide composites for efficient arsenate removal from drinking water, J. Hazard. Mater., 182 (2010).
[52] Z. Houg Huang, X. Zhang, W. Lv, M. Wang, Q.-H. Yang, F. Kang, Adsorption of lead(Ii) ions from aqueous solution on low_temperature exfoliated graphene nanosheets, Langmuir, 27 (2011) 7558–7562.
[53] S. Jinamoni, S. Goswami Archana, Study of the removal of toxic anions from contaminated water utilizing natural kaolinite clay of Assam, (IJRCE), 2 (2011) 92–96.
[54] K.Y. Foo, B.H. Hameed, Insights into the modeling of adsorption isotherm systems, Chem. Eng. J., 156 (2010) 2–10.
[55] B. Yu, J. Xu, J.-H. Liu, S.-T. Yang, J. Luo, Q. Zhou, J. Wana, R. Liao, H. Wang, Y. Liu, Adsorption behavior of copper ions on graphene oxide–chitosan aerogel, J. Environ. Chem. Eng., (2013).
[56] A.A. Inyinbor, F.A. Adekola, G.A. Olatunji, Kinetics, isotherms and thermodynamic modeling of liquid phase adsorption of Rhodamine B dye onto Raphia hookerie fruit epicarp, Water Res. Ind., 15 (2016) 14–27.
[57] N. Öztürk, T.E.l. Bektaş, Nitrate removal from aqueous solution by adsorption onto various materials, J. Hazard. Mater., 112 (2004) 155–162.
[58] S.H. Lin, C.L. Wu, Removal of nitrogenous compounds from aqueous solution by ozonation and ion exchange, Water Res., 30 (1996) 1851–1857.
[59] D. Forman, S. Al-Dabbagh, R. Doll, Nitrates, nitrites and gastric cancer in Great Britain, Nature, 313 (1985) 620–625.
[60] A. Afkhami, T. Madrakian, Z. Karimi, The effect of acid treatment of carbon cloth on the adsorption of nitrite and nitrate ions, J. Hazard. Mater., 144 (2007) 427–431.
[61] H.T. Banu, S. Meenakshi, Synthesis of a novel quaternized form of melamine–formaldehyde resin for the removal of nitrate from water, J. Water Process Eng., 16 (2017) 81–89.
[62] K. Chauhan, J. Kaur, P. Singh, P. Sharma, P. Sharma, G.S. Chauhan, An efficient and regenerable quaternary starch for removal of nitrate from aqueous solutions, Ind. Eng. Chem. Res., 55 (2016) 2507–2519.